Imperial College London

MSc Thesis

$\mathcal{PT}$-Symmetric Optical Lattices

Author:

Graham D. Hesketh

Supervisor:

Dr. Hugh F. Jones

September 24, 2010

Contents

$\mathcal{PT}$-Symmetric Optical Lattices

G. D. Hesketh

Physics Department, Imperial College, London SW7, London, UK

September 2010

Abstract

A brief overview of $\mathcal{PT}$-symmetric non-Hermitian Hamiltonians is presented and their realisation in optical lattices is discussed. A review of the literature is performed, accompanied by MATLAB and Maple simulations throughout. $\mathcal{PT}$-symmetric optical lattices are found to exhibit novel features with no analog in real-potential systems. These include band merging, nonreciprocity, power oscillations, double refraction and phase transitions. Following private communication with Dr. H. F. Jones, an equivalent Hamiltonian is presented for the $\cos(x)^2 + iV_0 \sin(2x)$ potential, and a dependence on the sinusoidal shape of the potential is noted in the double refraction. Soliton solutions are found in nonlinear $\mathcal{PT}$ lattices, and their instability is found to increase with non-Hermiticity parameter V_0.

1 Introduction

It is known that a physical quantum theory must adhere to a number of axioms. These include a real energy spectrum that is bounded below, a Hilbert space spanned by state vectors that in conjunction with an appropriate inner product insures a positive norm and a unitary time evolution operator that results in the

conservation of probability. In the Universe in which we live it is apparent that measurements of physical observables yield real quantities. In quantum mechanics these observables correspond to the eigenvalues of operators, and the reality requirement of observables demands that the eigenvalues of all operators be real quantities. In the case of the Hamiltonian operator, $\hat{H}$, the real eigenvalues correspond to a real energy spectrum. In order to provide a real spectrum it was postulated that all observables corresponded to the eigenvalues of Hermitian (self adjoint) operators and indeed, a Hermitian Hamiltonian not only ensures that the energy spectrum is real but it also takes care of the unitary temporal evolution.
In recent years Bender *et al.* conducted work that sought to continue quantum mechanics into the complex plane[1]. In particular they explored the spectra of non-Hermitian Hamiltonians and found that in fact many non-Hermitian Hamiltonians can produce entirely real spectra provided they possess something known as $\mathcal{PT}$ (parity-time) symmetry. The work of Bender *et al.* demonstrated that in many cases a threshold exists in the Hamiltonians, above which the spectrum is no longer completely real and instead becomes complex. This threshold marks the boundary between the $\mathcal{PT}$-symmetric and broken-symmetry phases and the transition is thus referred to as spontaneous $\mathcal{PT}$-symmetry-breaking ($\mathcal{PT}$-symmetry breaking has since found application in, amongst other things, quantum field theory, complex Lie Algebras and lattice QCD)[2].

1.1 $\mathcal{PT}$-Symmetry

The Hermiticity condition imposed on the Hamiltonian in conventional quantum mechanics is replaced in non-Hermitian Hamiltonian theory by the $\mathcal{PT}$-symmetric condition. The actions of the parity, $\hat{P}$, and time, $\hat{T}$, operators are defined as follows:

$$\hat{P}:\ \hat{p}\to-\hat{p},\ \hat{x}\to-\hat{x},\qquad \hat{T}:\ \hat{p}\to-\hat{p},\ \hat{x}\to\hat{x},\ i\to-i, \tag{1}$$

where $\hat{p}$ and $\hat{x}$ are the momentum and position operators, respectively. In general we define the Hamiltonian, $\hat{H}$, as $\hat{H} = \hat{p}^2/m + V(\hat{x})$, where m is the mass and V the potential. A Hamiltonian is defined as $\mathcal{PT}$-symmetric if it shares the same eigenfunctions as the $\hat{P}\hat{T}$ operator and satisfies the following condition[3]:

$$\hat{P}\hat{T}\hat{H} = \hat{H}\hat{P}\hat{T} \tag{2}$$

If the above condition is satisfied but the Hamiltonian does not share its eigenfunctions with the $\hat{P}\hat{T}$ operator then the Hamiltonian is considered to possess broken $\mathcal{PT}$ symmetry.

1.2 Orthogonality/Orthonormality of the Eigenfunctions of the $\mathcal{PT}$-Symmetric Hamiltonian and the $\mathcal{CPT}$ Inner Product

After specifying a Hamiltonian we may construct the time-independent Schrödinger equation and find the associated eigenvalues, E_n, and the corresponding eigenfunctions, $\psi_n(x)$, where n labels the n^{th} energy level (or band). These calculations are often only possible numerically (e.g. using the Runge-Kutta method) with analytic solutions available for only a limited number of cases. In order to express any state vector in the Hilbert space as a sum of eigenstates of the Hamiltonian we require the set of eigenfunctions to be orthonormal and complete.

1.2.1 Orthogonality

For a conventional Hermitian Hamiltonian the eigenfunctions are orthogonal with respect to the Hermitian inner product:

$$(\psi, \phi) = \int \psi(x)^* \phi(x)\, dx \tag{3}$$

Orthogonality means that for distinct eigenvalues $E_n \neq E_m$ the inner product vanishes, $(\psi_n(x), \phi_m(x)) = 0$. However, two eigenfunctions may be orthogonal with respect to one inner product but not with respect to another. The eigenfunctions of the non-Hermitian Hamiltonians are not in general orthogonal with respect to the standard Hermitian conjugate inner product, and consequently if we are to construct a successful quantum theory using the non-Hermitian Hamiltonian we must seek a new definition for the inner product. Bender *et al.* first discussed the possibility of using the $\mathcal{PT}$ inner product:

$$(\psi, \phi) \equiv \int_C \psi(x)^{\mathcal{PT}} \phi(x)\, dx = \int_C \psi(-x)^* \phi(x)\, dx \tag{4}$$

where C is an appropriate contour in the complex plane[4].Through integration by parts of the Schrödinger equation it can be shown that the eigenfunctions of the $\mathcal{PT}$ symmetric Hamiltonian associated with distinct eigenvalues are indeed orthogonal with respect to this inner product; however, this definition fails to insure a positive norm. In fact the algebraic sign of the norm of $\phi_n(x)$ using this inner product is $(-1)^n$, and it is possible to normalize the eigenfunctions so that this is the exact norm. However, the problem now is how to interpret these negative norm states. This definition of the inner product demonstrates that in fact half of the states will have negative norm. This in fact indicates a symmetry of the Hamiltonian and that symmetry is represented by the $\hat{C}$ operator.

1.2.2 Orthonormality and the $\mathcal{CPT}$ Inner Product

In order to enforce positive orthonormality for the eigenfunctions the $\mathcal{CPT}$ inner product. The additional operator, $\hat{C}$, is in some ways similar to the charge conjugation operator, hence its name. Furthermore, $\hat{C}$ is a linear operator that commutes with $\hat{H}$. The $\hat{C}$ operator can be written in coordinate space as a sum

over the $\mathcal{PT}$ normalized eigenfunctions of the $\mathcal{PT}$-symmetric Hamiltonian:

$$\mathcal{C}(x,y) = \sum_{n=0}^{\infty} \phi_n(x)\phi_n(y) \tag{5}$$

The $\mathcal{CPT}$ inner product is then defined as:

$$\langle \psi, \phi \rangle^{\mathcal{CPT}} \equiv \int_C \psi(x)^{\mathcal{CPT}} \phi(x)\, dx \tag{6}$$

where $\psi(x)^{\mathcal{CPT}} = \int \mathcal{C}(x,y)\phi(y)\, dx$. When dealing with non-Hermitian Hamiltonians one must first solve for the eigenstates of the Hamiltonian in order to know the $\hat{C}$ operator and in turn the inner product. This dynamic determination of the inner product differs from standard quantum mechanics where the Hilbert space and inner product are known even before selecting the Hamiltonian. The $\hat{C}$ operator has eigenvalues of ± 1 and it indicates the measured sign of the $\mathcal{PT}$ norm of an eigenstate. As a result this inner product is positive definite, as states with negative norm are multiplied by -1 when acted on by the $\hat{C}$ operator. The completeness relation has been derived for the $\mathcal{PT}$ conjugate case and a mathematical proof has been found[5]. In terms of the $\mathcal{CPT}$ conjugate it can be written as:

$$\sum_{n=0}^{\infty} \phi_n(x)[\mathcal{CPT}\phi_n(y)] = \delta(x-y) \tag{7}$$

1.2.3 Unitary Temporal Evolution with $\mathcal{PT}$-Symmetric Hamiltonians

In any quantum theory the temporal evolution of a state is given as:

$$\psi_t(x) = e^{-iHt}\psi_0(x) \tag{8}$$

To insure the norm remains unchanged in time, the temporal evolution must be unitary. In theories with $\mathcal{PT}$-symmetric Hamiltonians this remains true, as the $\mathcal{CPT}$ operator commutes with the Hamiltonian within the $\mathcal{CPT}$ inner product.

1.3 Mostafazadeh and Quasi and Pseudo-Hermiticity

In 2002 Mostafazadeh showed that all Hamiltonians with real spectra are pseudo-Hermitian [19], and that the $\mathcal{PT}$ Hamiltonians being considered were also pseudo-Hermitian (in fact he argued that as $\mathcal{PT}$-symmetry is neither a neccessary or sufficient condition for real eigenspectra, it is perhaps unrelated to the reality of the eigenspectrum). Pseudo-Hermitian Hamiltonians satisfy the condition:

$$H^\dagger = \eta H \eta^{-1} \tag{9}$$

where η is a positive definate Hermitian operator. $\mathcal{PT}$-symmetric Hamiltonians are a subclass of pseudo-Hermitian Hamiltonians with $\eta = PC$. When the CP operator is given as an exponential, $CP = e^{-Q}$ with Q Hermtian [2], η can be expressed as:

$$\eta = e^{-Q} \tag{10}$$

A Quasi-Hermitian Hamiltonian is one that is related to a Hermitian Hamiltonian, h, by a similarity transformation:

$$H = \rho^{-1} h \rho \tag{11}$$

where ρ is again Hermitian and positive definate. It is then seen that $\eta = \rho^2$ and thus, the similarity transformation that relates the Hamiltonian, H, to it's Hermitian equivalent is:

$$h = e^{-1/2Q} H e^{1/2Q} \tag{12}$$

It is generaly difficult to solve equation (12) however, and Hermitian equivalents cannot easily be found.

1.4 $\mathcal{PT}$-Symmetric Optical Structures: A testing ground for the Schrödinger equation

The work of Bender *et al.* demonstrated that the energy spectrum of a non-Hermitian Hamiltonian is in fact real if the Hamiltonian is $\mathcal{PT}$-symmetric. In 2007 D.N. Christodoulides *et al.* released a paper in which they suggested complex $\mathcal{PT}$-symmetric structures could be realized within an optical framework, and in particular through the paraxial theory of diffraction. In this optical model the dynamics are governed by Schrödinger-like equations in which the propagation distance, z, plays the part of time in quantum mechanics. Optical array constructions using real potentials have been considered in semiconductors, glasses and liquid crystals[6] and prior to $\mathcal{PT}$-symmetric optical considerations complex potentials were reviewed in both theoretical[7] and experimental optics[8]. $\mathcal{PT}$ symmetry in optical structures with complex periodic potentials is therefore, a natural extension. In order to be $\mathcal{PT}$ symmetric it is necessary (but not sufficient) to impose the condition on $\hat{H}$ that it commutes with the $\mathcal{PT}$ operator. This in turn places a constraint on the potential as:

$$\hat{H}\hat{P}\hat{T} = \hat{p}^2/m + V(x) \tag{13}$$

$$\hat{P}\hat{T}\hat{H} = \hat{p}^2/m + V^*(-x) \tag{14}$$

$$\hat{P}\hat{T}\hat{H} = \hat{H}\hat{P}\hat{T}, \tag{15}$$

which implies:

$$V(x) = V^*(-x) \tag{16}$$

In other words the real part of the potential must be an even function and the imaginary part an odd function of position, x. Christodoulides *et al.* suggested that this situation could be realized in optics by "involving symmetric index guid-

ing and an antisymmetric gain/loss profile"[9]. In optics the refractive index $n(x)$ plays the part of the potential, and for the system to be $\mathcal{PT}$-symmetric it must satisfy:

$$n(x) = n^*(-x) \tag{17}$$

The complex refractive index distribution, $n(x)$, may be split into a sum of its real and imaginary parts and a constant substrate background index, n_0:

$$n(x) = n_0 + n_R(x) + in_I(x) \tag{18}$$

If the Hamiltonian is $\mathcal{PT}$-symmetric the refractive-index profile, $n_R(x)$, is then an even function and the gain/loss distribution, $n_I(x)$, an odd function of position.

1.4.1 Derivation of the Schrödinger-like Beam Dynamics

The equation for an electromagnetic wave in a non-magnetic medium with no free charges or free currents and in Gaussian units is:

$$\vec{\nabla} \times \left(\vec{\nabla} \times \vec{E}(\vec{x}, z, t)\right) + \frac{1}{c^2}\partial_t^2 \vec{E}(\vec{x}, z, t) = -\frac{4\pi}{c^2}\partial_t^2 \vec{P}(\vec{x}, z, t) \tag{19}$$

where $\vec{P}(\vec{x}, z, t)$ is the total material polarization and the transverse coordinates have been compiled into the vector, $\vec{x}$. Consider, then, the single-frequency component of the electric field:

$$\vec{E}(\vec{x}, z, t) = \vec{E}(\vec{x}, z)e^{-i\omega t} + c.c,$$

where ω is the angular frequency of the oscillation. In general the polarization vector $\vec{P}$ is expanded as a power series in the electric field $\vec{E}$. For linear materials, however, we may exclude higher order terms and make use of the constitutive

relation:

$$4\pi\vec{P} = (n^2 - 1)\vec{E} \tag{20}$$

We then, after implementing the vector identity for the curl of the curl of a vector, obtain:

$$\vec{\nabla}\left(\vec{\nabla}\cdot\vec{E}\right) - \nabla^2\vec{E} - \frac{\omega^2}{c^2}n^2(\vec{x}, z, \omega, \vec{E}; t)\vec{E} = 0$$

In the absence of free charges the divergence of $\vec{E}$ vanishes; thus we reach the homogeneous vector Helmholtz equation in the form:

$$[\nabla^2 + \frac{\omega^2}{c^2}n^2(\vec{x}, z, \omega, \vec{E}; t)]\vec{E}(\vec{x}, z) = 0 \tag{21}$$

For a constant polarization vector we may reduce the homogeneous vector Helmholtz to the scalar equation. Furthermore, in the systems which form the focus of this study the field will not be a function of y and the refractive index will generally be a function of x only. If then we make the following substitution:

$$n^2(\vec{x}, z, \omega, \vec{E}; t) = (n_0 + \delta n(x))^2 \approx n_0^2 + 2n_0\delta n(x)$$

where we have taken $\delta n(x) \ll n_0$, equation (21) reduces to:

$$[\partial_x^2 + \partial_z^2 + k_0^2 + 2\frac{k_0^2}{n_0}\delta n(x)]E(x, z) = 0 \tag{22}$$

where $k_0 = n_0\omega/c$. The electric field may be written as an envelope function times a plane wave propagating along z: $E(x, z) = \psi(x, z)e^{ik_0 z}$. Taking this into account

we may recast equation (22) as:

$$[\partial_x^2 + \partial_z^2 + 2ik_0\partial_z + 2\frac{k_0^2}{n_0}\delta n(x)]\psi(x,z) = 0 \tag{23}$$

Now we employ the slowly-varying envelope approximation known as the "paraxial approximation". To do this we introduce new rescaled co-ordinates:

$$X = \frac{x}{x_0}$$
$$Z = \frac{z}{2kx_0^2}$$

In terms of these new co-ordinates equation (23) becomes:

$$[\partial_X^2 + \epsilon^2\partial_Z^2 + i\partial_Z + 2\frac{k_0^2}{n_0}x_0^2\delta n(X)]\psi(X,Z) = 0 \tag{24}$$

where $\epsilon = 1/(2kx_0)$. The transverse length scale, x_0, is naturally set by the spot radius of a laser or size of an aperture, and provided it is much greater than the wavelength, $\epsilon \ll 1$ and the ∂_Z^2 term may be dropped. This is known as the paraxial approximation. Equation 24 then becomes:

$$[\partial_X^2 + i\partial_Z + V(X)]\psi(X,Z) = 0 \tag{25}$$

with $V(X) = 2\frac{k_0^2}{n_0}x_0^2\delta n(X)$. This of course is the well known 1d Schrödinger equation with Z playing the role of time.

2 $\mathcal{PT}$-Symmetry in a Coupled 2-Channel Optical System

2.1 Experimental Realization of $\mathcal{PT}$-Symmetry in a Linear Coupled 2-Channel Optical System

Following the 2007 paper by Christodoulides *et al.* on the "Theory of coupled optical $\mathcal{PT}$-symmetric structures"[9], attentions turned to the experimental realization. In 2010 three of the authors of the theoretical 2007 paper, Christodoulides, K.G. Makris and R. El-Ganainy, together with M. Segev and D. Kip, published an article in Nature detailing the first experimental observation of a $\mathcal{PT}$-symmetric optical system with a complex potential[10]. In addition to this, the group also witnessed $\mathcal{PT}$-symmetry breaking and asymmetric power oscillations. The importance of the work was explained by the group:

> Our results may pave the way towards a new class of PT-symmetric materials with intriguing and unexpected properties that rely on non-reciprocal light propagation and tailored transverse energy flow[10].

The ultimate goal was to consider periodic optical systems but first it was necessary to establish the $\mathcal{PT}$ properties of a single cell. Christodoulides *et al.* achieved this through the construction of a coupled system with two channels, one of which would receive gain, γ_G, through optical pumping and the other only loss, γ_L. The electric envelope, E, of the optical beam, under the $\mathcal{PT}$ symmetric conditions laid out in (17), obeys the paraxial diffraction equation:

$$i\partial_z E + \frac{1}{2k_0 n_0}\partial_x^2 E + k_0[n_R(x) + in_I(x)]E = 0$$

where $k_0 = 2\pi/\lambda$ with λ the wavelength. The optical dynamics of the two coupled waveguides is then:

$$i\frac{dE_1}{dz} - i\frac{\gamma_{Geff}}{2}E_1 + \kappa E_2 = 0, \quad i\frac{dE_2}{dz} + i\frac{\gamma_{Geff}}{2}E_2 + \kappa E_1 = 0 \tag{26}$$

with $E_{1,2}$ the field amplitudes in the respective channels, $\kappa = \pi/2L_c$ the coupling constant, with coupling length L_c, and $\gamma_{Geff} = \gamma_G - \gamma_L$ the effective gain. For a $\mathcal{PT}$-symmetric system we require $\gamma_{Geff} = \gamma_L = \gamma$. The $\mathcal{PT}$-symmetric coupled equations can be written in matrix form using the non-Hermitian Hamiltonian:

$$i\frac{d}{dz}\begin{bmatrix} E_1(z) \\ E_2(z) \end{bmatrix} = H \begin{bmatrix} E_1(z) \\ E_2(z) \end{bmatrix} \tag{27}$$

$$H = \begin{bmatrix} \frac{1}{2}i\gamma & -\kappa \\ -\kappa & \frac{1}{2}i\gamma \end{bmatrix} \tag{28}$$

This has solution:

$$\begin{bmatrix} E_1(z) \\ E_2(z) \end{bmatrix} = e^{-iHt} \begin{bmatrix} E_1(0) \\ E_2(0) \end{bmatrix} \tag{29}$$

which leads to the following expressions for the electric field $E_{1,2}(z)$ as a function of the initial states, $E_1(0)$ and $E_2(0)$:

$$E_1(z) = \left(\cosh\left(1/2\,\xi(z)\right) + \frac{\gamma\, z \sinh\left(1/2\,\xi(z)\right)}{\xi(z)}\right) E_1(0) + \frac{2\,iz\sinh\left(1/2\,\xi(z)\right)\kappa}{\xi(z)} E_2(0) \tag{30}$$

$$E_2(z) = \left(-\cosh\left(1/2\,\xi(z)\right) + \frac{\gamma\, z \sinh\left(1/2\,\xi(z)\right)}{\xi(z)}\right) E_2(0) + \frac{2\,iz\sinh\left(1/2\,\xi(z)\right)\kappa)}{\xi(z)} E_1(0) \tag{31}$$

with $\xi(z) = \sqrt{z^2(-4\kappa^2 + \gamma^2)}$. The $\mathcal{PT}$-symmetric threshold is reached at $\gamma = 2\kappa$. Below this value the eigenvectors and corresponding eigenvalues (right) are given as:

$$|1,2\rangle = (1, \pm e^{\pm i\theta}), \quad \pm\cos(\theta) \tag{32}$$

where $\sin(\theta) = \gamma/2\kappa$. At threshold they coalesce to:

$$|1,2\rangle = (1, i) \tag{33}$$

Finally above threshold where $\cosh(\theta) = \gamma/2\kappa$ they are given as:

$$|1,2\rangle = (1, ie^{\mp\theta}), \quad \mp i\sinh(\theta) \tag{34}$$

It is noted that the eigenstates of this system are *not* orthogonal. In a Hermitian system, $\gamma = 0$, superposition of the symmetric and antisymmetric eigenstates results in reciprocal wave propagation. For the $\mathcal{PT}$-symmetric system the basis is skewed, resulting in non-reciprocal dynamics and power oscillations. By switching the input channel from 1 to 2, $(E_1(0) = 1, E_2(0) = 0) \rightarrow (E_1(0) = 0, E_2(0) = 1)$, an entirely different output state is obtained. As we exceed threshold this situation becomes increasingly more evident. Above threshold the eigenvalues are complex, which results in an exponential increase (or decrease) in amplitude in channel 1 (or 2). Interestingly, this results in light predominantly exiting the system in channel 1 irrespective of the input state.

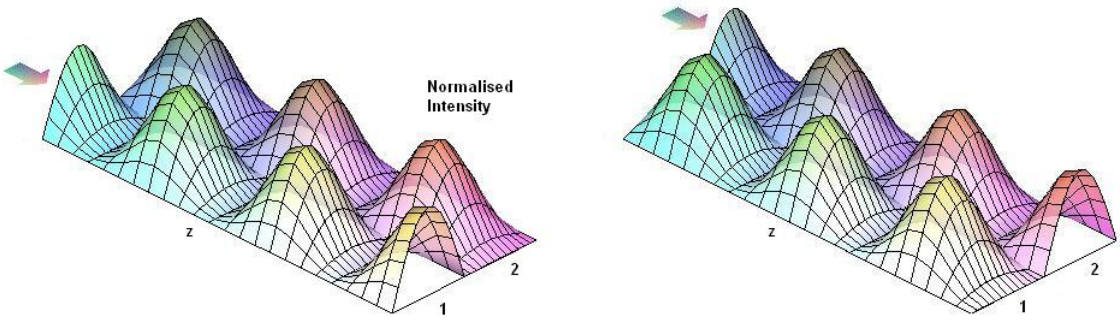

Figure 1: Normalised intensity in the 2 channels. Conventional system ($\gamma = 0$) is reciprocal during excitation of channel 1 (left diagram) and channel 2 (right diagram).

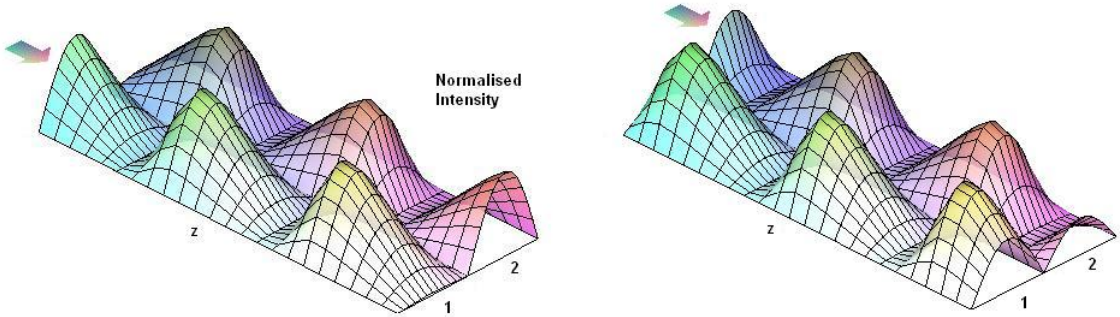

Figure 2: $\mathcal{PT}$-symmetric system below threshold ($\gamma = \kappa/2$) during excitation of channel 1 (left diagram) and channel 2 (right diagram). On close examination the system is non-reciprocal.

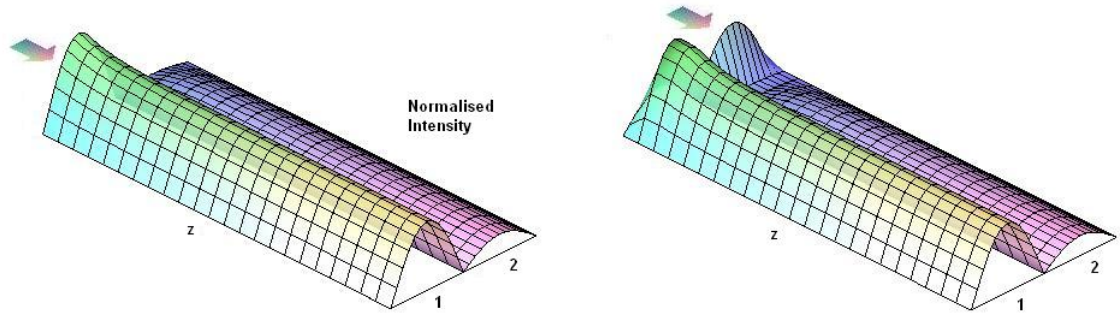

Figure 3: $\mathcal{PT}$-symmetric system above threshold ($\gamma = 1.2\kappa$) during excitation of channel 1 (left diagram) and channel 2 (right diagram). System is again non-reciprocal with light propagating mainly in channel 1 irrespective of the input state.

In addition, Christodoulides *et al.* measured the intensity distribution at the output, ($z = 2cm$), at different instants t. They assumed an exponential temporal build up in gain (proportional to the concentration of Fe^{3+} centres[10]) governed by the equation:

$$\gamma_G(T) = \gamma_{max}[1 - e^{-T}] \tag{35}$$

with $T = t/\tau$, t the time and τ the Maxwell time constant. With $\gamma_L = 2\kappa$, $\gamma_{max} = 5\kappa$ and for the optical system employed $\kappa = 1.9cm^{-1}$. From previous considerations of the $\mathcal{PT}$ symmetry we find:

$$\begin{aligned} \gamma_{Geff} &= \gamma_G - \gamma_L \\ \gamma_{Geff} &= \gamma_L = \gamma \\ \gamma &= \frac{\gamma_G}{2} = \frac{5}{2}\kappa[1 - e^{-T}] \end{aligned} \tag{36}$$

By inserting equation (36) into equations (30) and (31) we obtain expressions for the intensity $I_{1,2} = |E_{1,2}|^2$ as a function of time. The intensity was measured at the channel outputs at different instances and for different input states (Figure 4).

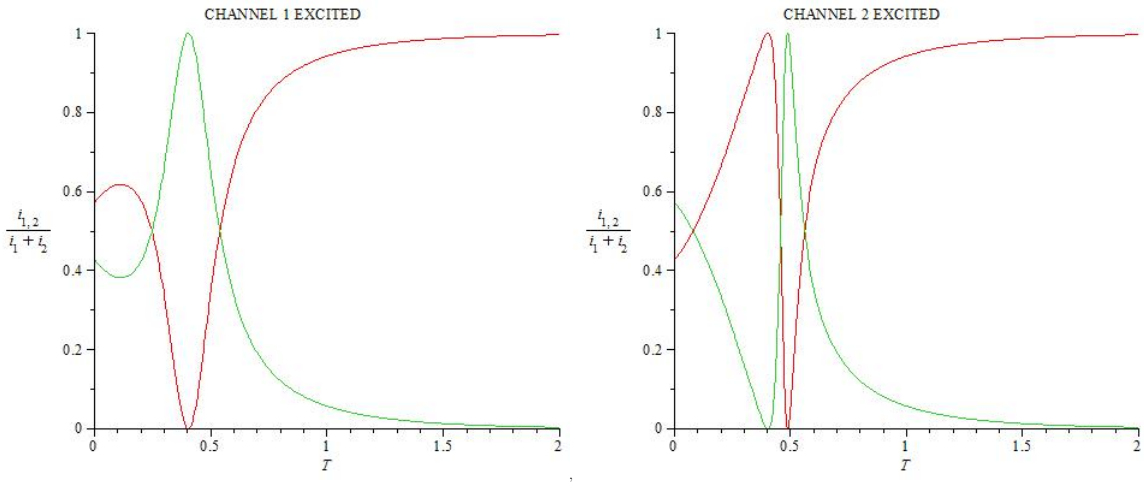

Figure 4: Analytic solutions of the (normalised) coupled equations for the intensity at the output. I_1 in green, I_2 in red. These simulations were run by the group and found to be in good agreement with expermental data.

2.2 Nonlinear $\mathcal{PT}$-Symmetric Coupled System

The work of Christodoulides *et al.* in the previous section examined exclusively the dynamics of the linear coupled optical system. It was natural of course to extend such considerations to include nonlinear behaviour. In May 2010 Hamidreza Ramezani and Tsampikos Kottas, together with Christodoulides and El-Ganainy, published a paper entitled *Unidirectional Nonlinear $\mathcal{PT}$-Symmetric Optical Structures* [11]. Prominent among the motivations of the paper was the possibility of being able to provide a means of unidirectional information flow in a manner that does not rely on the Faraday effect. The Faraday effect generally requires the use of materials that are incompatable with light emitting wafers[12]. In reference [11] non-reciprocal $\mathcal{PT}$-symmetric dynamics are combined with nonlinear self-trapping phenomena[13] and the outcome is directed dynamics that could be utilised in optical isolators or diodes. The system under consideration is similar to that of the linear case in the previous section. Two $\mathcal{PT}$-symmetric coupled waveguide elements are employed, only this time with Kerr nonlinearity strength, χ. Such $\mathcal{PT}$-symmetric nonlinear systems are easily realised on semiconductor wafers with Kerr-like properties[14].

In nonlinear materials the refractive index changes as it interacts with an electric field. In this case the applied electric field is the light itself as it propagates through the material. Owing to this modified potential we must in turn alter the equations governing the optical dynamics. For a nonlinear material the higher order terms in the expansion of the polarisation vector, $\vec{P}$, cannot be ignored and the constitutive relation (20) is no longer applicable. For nonlinear materials we approximate the expansion with 1st and 3rd order terms (The even-ordered terms in the expansion drop out if the material exhibits inversion symmetry). Consequently equation (20)

is replaced with:

$$4\pi\vec{P} = (n^2 - 1 + \chi|\vec{E}|^2)\vec{E} \tag{37}$$

with χ a measure of nonlinearity, and equation (25) then becomes the nonlinear Schrödinger-like equation[15]:

$$[\partial_X^2 + i\partial_Z + V(X) + \chi|\psi(x,z)|^2]\psi(X,Z) = 0 \tag{38}$$

In the Kerr nonlinear version of a coupled two-channel waveguide system the equations for the modal amplitudes are:

$$i\frac{d}{dz}\psi_1(z) + \psi_2(z) - i\gamma\psi_1(z) + \chi|\psi_1(z)|^2\psi_1(z) = 0 \tag{39}$$

$$i\frac{d}{dz}\psi_2(z) + \psi_1(z) + i\gamma\psi_2(z) + \chi|\psi_2(z)|^2\psi_2(z) = 0 \tag{40}$$

where γ is again the scaled gain/loss coefficient and χ is the strength of the Kerr nonlinearity. Both γ and χ are normalised in units of the coupling length. Equations (39) and (40) are not in general analytically solvable and thus numerical solutions are sought. With $\chi = 0$ we obtain the linear case of the preceding section. In the linear limit $\mathcal{PT}$-symmetry breaking occurs in equations (39) and (40) at γ=1. Nonlinearity will be explored here in the exact $\mathcal{PT}$-symmetric phase with $\gamma < 1$.

For $\gamma = 0$ there are analytic solutions to equations (39) and (40) in the form of elliptic functions[13]. If the initial state corresponds to stimulation of only one of the channels, either channel 1(gain channel) or channel 2 (loss channel), then for $\gamma = 0$ two distinct behaviours are observed. For $\chi < 4$ Rabi oscillations result in the beam oscillating between the channels, and for $\chi > 4$ self-trapping dynamics occurs, causing localization of the beam entirely in the channel of the initial state[13]. In both cases the beam dynamics are reciprocal as they were for

$\gamma = 0$ in the linear case.

For the interesting case of $\gamma \neq 0$ analytic solutions to (39) and (40) are in general unknown and instead the dynamics are explored through numerical integration. With $\gamma = 0.1$ two examples are provided, $\chi = 1.9$ and $\chi = 8$. The dynamics is non-reciprocal for $\gamma \neq 0$, and this is particularly evident for the $\chi = 8$ case where the beam exits channel 1 (gain) regardless of the input state. The intensity in channel 2 (loss) is seen to go exponentially to zero for waveguides longer than some critical value, z_d. It is this unidirectional property that could allow the system to be used as an optical isolator (diode).

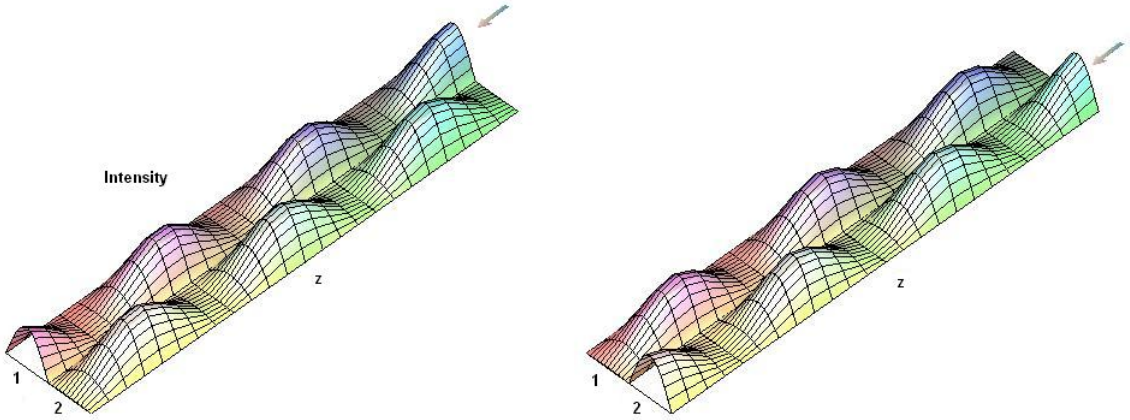

Figure 5: Field intensity in a nonlinear 2 channeled couple system for $\gamma = 0.1$ and nonlinearity strength $\chi = 1.9$ during excitation of channel 1 (left) and channel 2 (right). System is actually not quite reciprocal.

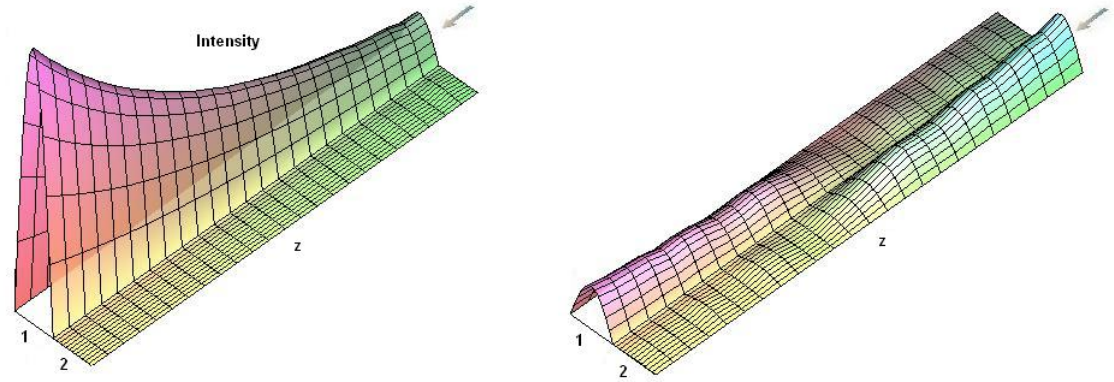

Figure 6: Field intensity in a nonlinear 2 channeled couple system for $\gamma = 0.1$ and nonlinearity strength $\chi = 8$ during excitation of channel 1 (left) and channel 2 (right). The nonreciprocity of the system is drastic, with light only exiting channel 1 regardless of input state.

3 $\mathcal{PT}$-Symmetric Optical Lattices

The investigation of $\mathcal{PT}$-symmetric optical lattices is of particular importance, as the interesting dynamics attributed to $\mathcal{PT}$-symmetry may feature in the synthesis of pseudo-Hermitian materials with novel optical properties. These properties were explored by the group K. G. Makris, R. El-Ganainy and D. N. Christodoulides in the paper *Beam Dynamics in $\mathcal{PT}$-Symmetic Optical Lattices* [16]. Once again the structure utilises a judicious gain/loss set up but now within the context of a complex $\mathcal{PT}$-symmetric array and we again focus on the diffraction dynamics of optical beams in the spatial domain. The refractive index is of the form (18):

$$n(x) = n_0 + n_R(x) + in_I(x)$$

The previous conditions imposed by the $\mathcal{PT}$-symmetry still apply, i.e.:

$$n_R(x) = n_R(-x), \quad n_I(x) = -n_I(x) \tag{41}$$

In a lattice set up, however, $n(x)$ is periodic such that:

$$n_{R,I}(x) = n_{R,I}(x + D) \tag{42}$$

with D the period of the lattice. The complex potential $V(x)$ is also periodic such that $V(x) = V(x + D)$. Under these conditions and with $n_{R,I}(x) \ll n_0$ the dynamics once again obeys the paraxial equation of diffraction which, after suitable rescaling, resembles the Schrödinger equation (25):

$$[\partial_X^2 + i\partial_Z + V(X)]\psi(X, Z) = 0$$

Such $\mathcal{PT}$-symmetric lattices may be realised in the visible and long wavelength regime when the gain or loss coefficients are appropriately selected[16].

3.1 Band Structure of a Periodic $\mathcal{PT}$-Symmetric Lattice

Crucial to the understanding of the $\mathcal{PT}$ lattice properties is the analysis of the band structure. Solutions of the form:

$$\psi(x,z) = \phi_{kn}(x)e^{i\beta_n(k)z} \tag{43}$$

are sought with $\phi_{kn}(x)$ the n-band Floquet-Bloch mode, k the Bloch momentum and $\beta_n(k)$ the associated eigenvalue (propagation constant). In all instances k is kept to within the first Brillouin zone $-\pi/D \leq k < \pi/D$. As mentioned in the introduction, a necessary but not sufficient condition imposed on the potential in order to insure a real eigenspectrum is:

$$V(x) = V^*(-x) \tag{44}$$

Focus is given here to the potential:

$$V(x) = 4(\cos^2(x) + V_0 i \sin(2x)) \tag{45}$$

with lattice period $D = \pi$.

3.1.1 Determining $\beta(k)$

By substituting equation (43) into the Schrödinger-like equation, (25), we find that the n-band Floquet Bloch modes, $\phi_{kn}(x)$, satisfy the time (or in this case z) independent Schrödinger equation:

$$[\frac{d^2}{dx^2} + V(x) - \beta_{kn}]\phi_{kn}(x) = 0 \tag{46}$$

There are two linear independent solutions to a second order differential equation that are defined by distinct initial conditions. We may reduce the order of the

differential system using the following substitutions:

$$\begin{aligned} \phi_{kn}(x) &= U(x) \\ \frac{d}{dx}\phi_{kn}(x) &= U'(x) \\ \frac{d}{dx}U(x) &= U'(x) \end{aligned} \tag{47}$$

Combining (46) and (47) we obtain the system:

$$\begin{aligned} \frac{d}{dx}U'(x) &= (-V(x) + \beta_{kn})U(x) \\ \frac{d}{dx}U(x) &= U'(x) \end{aligned} \tag{48}$$

which yields two solutions subject to the following different initial conditions:

$$(U(0) = 1,\ U'(0) = 0), \quad (U(0) = 0,\ U'(0) = 1) \tag{49}$$

Then, for a specific value of β_{kn} and for a specific function $V(x)$, these equations can be numerically solved on a computer using the Runge-Kutta method, for example.

There is a well-known relation between these solutions and the Bloch momentum k, (Floquet method), that is:

$$\cos(k\pi) = \frac{1}{2}(U_1(\pi) + U_2'(\pi)) \tag{50}$$

which enables us to determine k for a specified value of β_{kn}:

$$k(\beta) = \frac{1}{\pi}\arccos\left(\frac{1}{2}U_1(\pi) + \frac{1}{2}U_2'(\pi)\right) \tag{51}$$

Plotting a graph of $k(\beta)$ on its side, as if it were $\beta(k)$, thus produces the eigenspectrum, with physically meaningful values of k lying in the region $-1 \geq k \leq +1$.

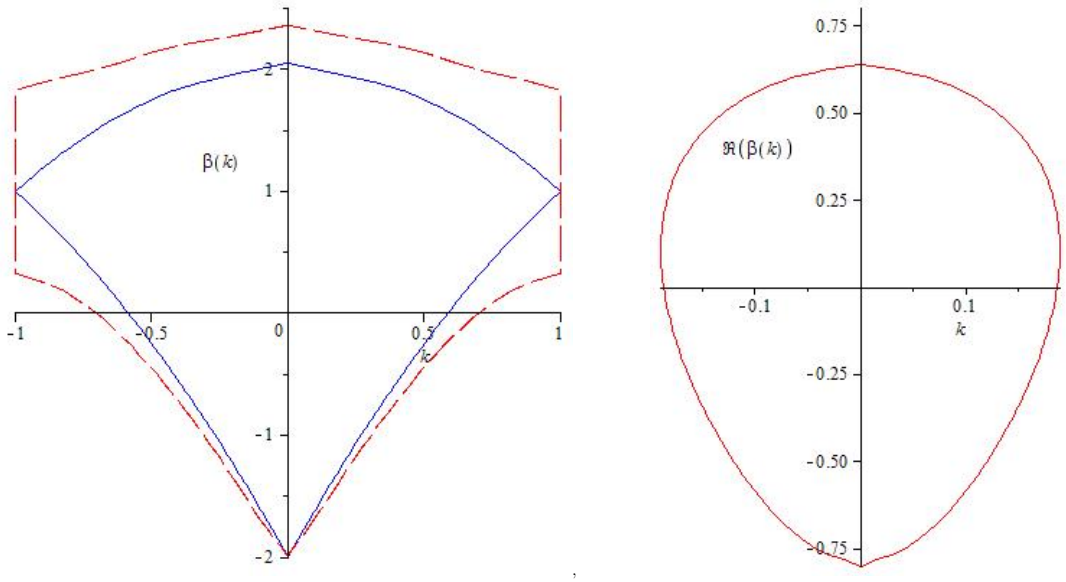

Figure 7: LEFT: First 2 bands for $V_0 = 0.3$ (red dashed line) and $V_0 = V_0^{th} = 0.5$ (blue line). RIGHT: Real part of first 2 bands for $V_0 = 0.85$. In this region the eigenvalue is real but outside it is complex.

The eigenvalue, β, is in general a complex number. In an exact $\mathcal{PT}$ phase where eigenfunctions of the PT operator are also eigenfunctions of the Hamiltonian, H, and where the PT operator and H commute, β is real valued. Above some threshold value, $V_0^{th}(x)$, eigenfunctions of the PT operator are no longer eigenfunctions of the Hamiltoninian, despite the fact that PT and H commute. The symmetry is then broken and β will no longer be completely real but will rather become complex.

For $V(x)$ given in equation (45) the threshold is found to be $V_0^{th} = 1/2$. Figure 7 (left) shows that for $V_0 = 0.3$ the forbidden gaps are open but for $V_0 = V_0^{th} = 0.5$ the first two bands close at $k = \pm 1$. For $V_0 = 0.85 > V_0^{th}$ the first two bands colide forming an oval-like structure (right). This double-valued band has a complex associated eigenspectrum but in the oval region it is real valued. For ever increasing values of V_0 more bands begin to merge together. The bands that don't merge, however, maintain their real eigenvalues[16].

3.2 Equivalent Hermitian Hamiltonian for non-Hermitian $A[\cos(x)^2 + iV_0 \sin(2x)]$ Potential

Through private communication with Dr. H. F. Jones, it has been noted that a Hermitian equivalent Hamiltonian exists for the non-Hermitian potential used in equation (45). For $V_0 < V_0^{th} = 0.5$ the potential presented in (45) may be rewritten as:

$$V(x) = 4[\cos^2(x) + iV_0 \sin(2x)] = 2 + 2\sqrt{(1 - 4V_0^2)\cos(2x - i\theta)}, \tag{52}$$

with $\theta = \text{arctanh}(2V_0)$ (For a similar transformation see reference [17]).
Consequently the Hamiltonian can be written as:

$$H = p^2 - 2 - 2\sqrt{(1 - 4V_0^2)\cos(2x - i\theta)}, \tag{53}$$

which, following the complex shift $x \to x + \frac{1}{2}i\theta$, becomes the Hermitian Hamiltonian:

$$h = p^2 - 2 - 2\sqrt{(1 - 4V_0^2)\cos(2x)} \tag{54}$$

The Hermitian, h, is related to the non-Hermitian Hamiltonian, H, through the similarity transformation:

$$h = e^{-\frac{1}{2}Q} H e^{\frac{1}{2}Q}, \tag{55}$$

with $Q = V_0 \vec{p}^2 \equiv -i\theta d/dx$. Consequently the eigenspectra of both Hamiltonians are identical below threshold. The Schrödinger-like equation then becomes the Mathieu equation[18]:

$$[\frac{d^2}{dx^2} + a - 2q\cos(2x)]\psi = 0, \tag{56}$$

with $q = -\sqrt{1-4V_0^2}$ and $a = -\beta$. The energy levels are then numericaly derived as for the previous non-Hermitian case.

Above threshold the corresponding identity is

$$V(x) = 4[\cos^2(x) + iV_0 \sin(2x)] = 2 + 2i\sqrt{(4V_0^2 - 1)\sin(2x - i\zeta)}, \tag{57}$$

with $\zeta = \text{arccoth}(2V_0)$. However the equivalent Hamiltonian, h, in this case is again non-Hermitian. In this region the corresponding Schrödinger-like equation is:

$$[\frac{d^2}{dx^2} + a + i\sqrt{(4V_0^2 - 1)}\sin(2x)]\psi = 0, \tag{58}$$

where shifting $x \to x - \pi/2$ again provides the Mathieu function but with pure imaginary q.

3.3 Floquet-Bloch Modes of a $\mathcal{PT}$-Symmetric Lattice

The Floquet-Bloch modes of a $\mathcal{PT}$-symmetric lattice also exhibit some strange features. For complex potentials the eigenfunctions are not seen to exhibit zero nodes at the edges of the Brillouin zone. In addition, different modes with the same eigenvalue, $\beta(k)$, are found to be complex conjugate pairs. In real lattices the mode at k is conjugate to that at $-k$, yet in a $\mathcal{PT}$ lattice this is not the case. For a $\mathcal{PT}$-symmetric lattice:

$$\phi_{kn}(x) \neq \phi_{-kn} * (x) \tag{59}$$

Consequently the band structure is said to be nonreciprocal with respect to k for a $\mathcal{PT}$-symmetric potential. This in fact follows from the nonorthogonality of the Floquet-Bloch modes of a $\mathcal{PT}$ system. The orthogonality relation for the modes of a real system is no longer valid, that is in a $\mathcal{PT}$ system[16]:

$$\int_{-\infty}^{+\infty} \phi^*_{k'm}(x)\phi_{kn}(x)dx \neq \delta_{n,m}\delta(k-k') \tag{60}$$

As a result the inner product needs to be modified if it is to project arbitrary input waves onto the skewed $\mathcal{PT}$-symmetric eigenmode basis. In fact in an infinite $\mathcal{PT}$ lattice the orthogonality condition is given as:

$$\int_{-\infty}^{+\infty} \phi^*_{k'm}(x)\phi_{kn}(x)dx = \frac{2\pi}{D} d_{kn}\delta_{n,m}\delta(k-k') \tag{61}$$

This orthogonality relation is significantly different. Here both k and x are reflected about the axis of symmetry.

3.4 Double Refraction and Power Oscillations

The aspects of $\mathcal{PT}$-symmetry that are of most interest in an optical lattice are those associated with the dynamic beam evolution. Figure 8 shows wide beam excitation of a $\mathcal{PT}$-symmetric lattice with $V_0 = 0$ (Hermitian), and $V_0 = 0.49$ (non-Hermitian). In the $\mathcal{PT}$ case with $V_0 = 0.49$, the beam is seen to split in two. This is known as double refraction. This behaviour is attributed to the skewness of the Floquet-Bloch modes which leads to an assymetric distribution of the modal coefficients in k space[16]. For an input signal projected onto the orthogonal Floquet-Bloch basis these coefficients indicate the mode occupancy in the n^{th} band for Bloch momentum k. Moreover, the beam propogation will follow the gradient $\nabla_k(\beta)$, thus, Figure 8 can be intuitively understood as the promotion of energy flow from left to right by the gain/loss dipoles.

Figure 9 demonstrates once more the nonreciprocity of a $\mathcal{PT}$ lattice. For $V_0 = 0.45$, and incident angles $\theta = \pm 2$, the intensity evolution of a wide beam excitation is displayed. The plots are different, however, for the respective angles and thus, the system is seen to distinguish right from left. This effect is again a result of the skewed modes[16].

The dynamics also feature notable oscillations in power with, z. In a $\mathcal{PT}$-symmetric lattice the conserved quantity is Q, the quasi power and it is defined as:

$$Q = \int_{-\infty}^{+\infty} E(x,z)E^*(-x,z)dx \tag{62}$$

with $E(x,z)$ the input field. In fact the actual power $P = \int_{-\infty}^{+\infty} |E(x,z)|^2 dx$ is not conserved, but instead oscillates during propogation. This oscillation is a consequence of the unfolding of the skewed Floquet-Bloch modes[16], and is most obvious in Figure 10 where a single channel is excited for the same values of V_0 used in Figure 8. In this case secondary emissions are seen to occur.

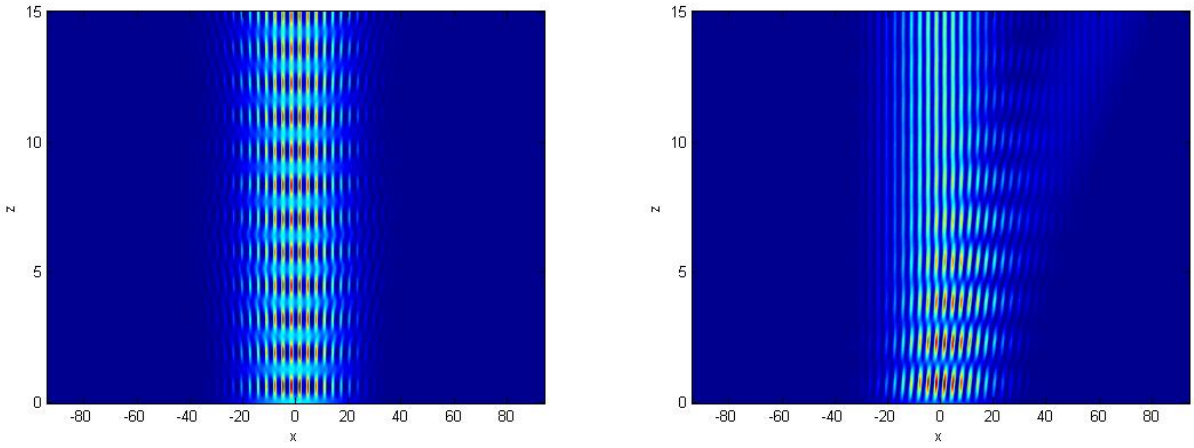

Figure 8: Intensity as a function of x and z for wide beam excitation at normal incidence. LEFT: $V_0 = 0$ (Hermitian) RIGHT: $V_0 = 0.49$ (non-Hermitian). System demonstrates double refraction.

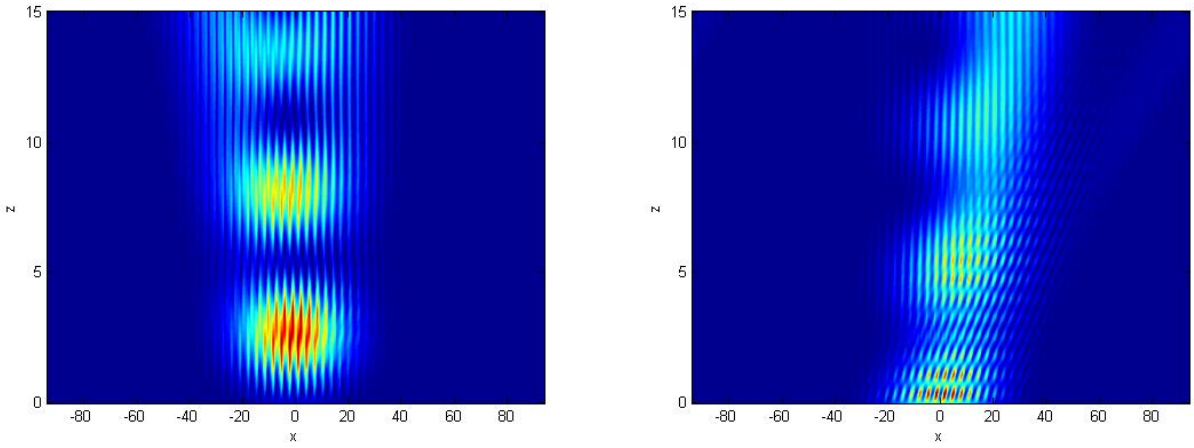

Figure 9: Wide beam angled excitation with $V_0 = 0.45$. LEFT: $\theta = 2^o$ RIGHT: $\theta = -2^o$. System demonstrates nonreciprocity.

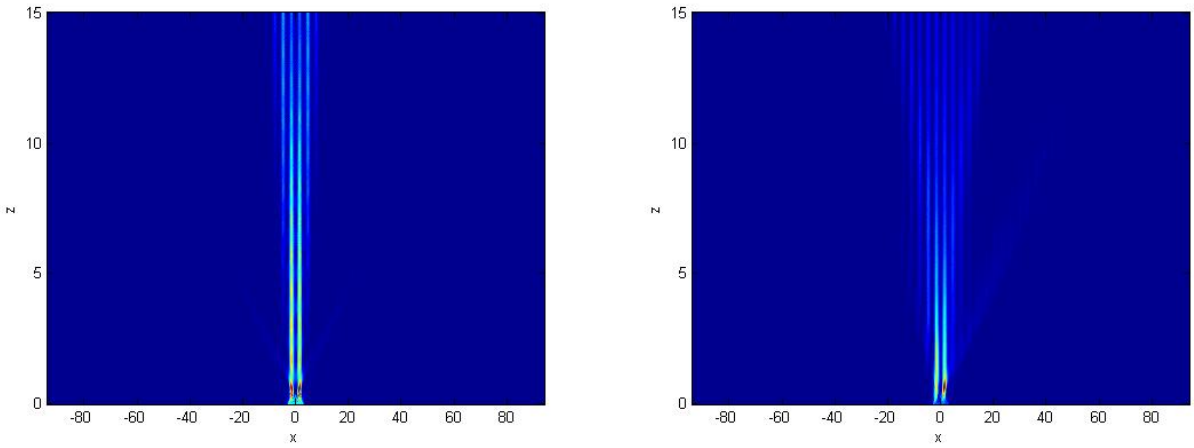

Figure 10: Single channel excitation. LEFT: $V_0 = 0$ (Hermitian) RIGHT: $V_0 = 0.49$ (non-Hermitian). System demonstrates power oscilations with secondary emissions.

3.5 The Dependence of Double Refraction on the Sinusoidal Shape of the Potential

In the previous section the phenomena of double refraction was identified in $\mathcal{PT}$ lattices. In Figure 8 the splitting of the beam was shown for the potential $V(x) = 4[\cos^2(x) + iV_0 \sin(2x)]$ with $V_0 = 0.49$. It has been noted by Dr. H. F. Jones, and presented here following private communication, that this effect is heavily dependent on the sinusoidal shape of the potential. Figure 11 demonstrates that as the shape of the real and imaginary parts of the potential tend from sinusoidal functions to square wave functions, the double refraction dissapears. It is not known why this phenomena occurs. The changing shape of the potential in Figure 11 is implemented in MATLAB by the elliptic function:

$$W(x) = -2ellipj((\frac{4x}{\pi} - 1)ellipke(\xi), \xi) + 4iV_0 ellipj((\frac{4x}{\pi} ellipke(\xi), \xi) \qquad (63)$$

where *ellipj* is the Jacobi elliptic function and *ellipke* is the elliptic integral of the first kind. The Jacobi elliptic function is parameterized by ξ which takes values $0 < \xi \leq 1$. For $\xi = 0$, $W(x) = V(x/2)$ and as ξ tends to 1 the function $W(x)$ becomes more square. The Jacobi elliptic function spreads out as the value of it's argument increases. The 2π periodicity is preserved here through the inclusion of the elliptic integral in the argument. The function *ellipj* returns the Jacobi elliptic function $sn(u, \xi) = sin(\Phi)$ and is defined[18] according to:

$$u = \int_0^{\Phi} \frac{d\theta}{\left(1 - \xi \sin^2 \theta\right)^2} \qquad (64)$$

The function *ellipke* returns the complete elliptic integral $K(\xi)$ defined[18] as:

$$K(\xi) = \int_0^1 \frac{1}{\sqrt{(1 - t^2)(1 - \xi t^2)}} dt \qquad (65)$$

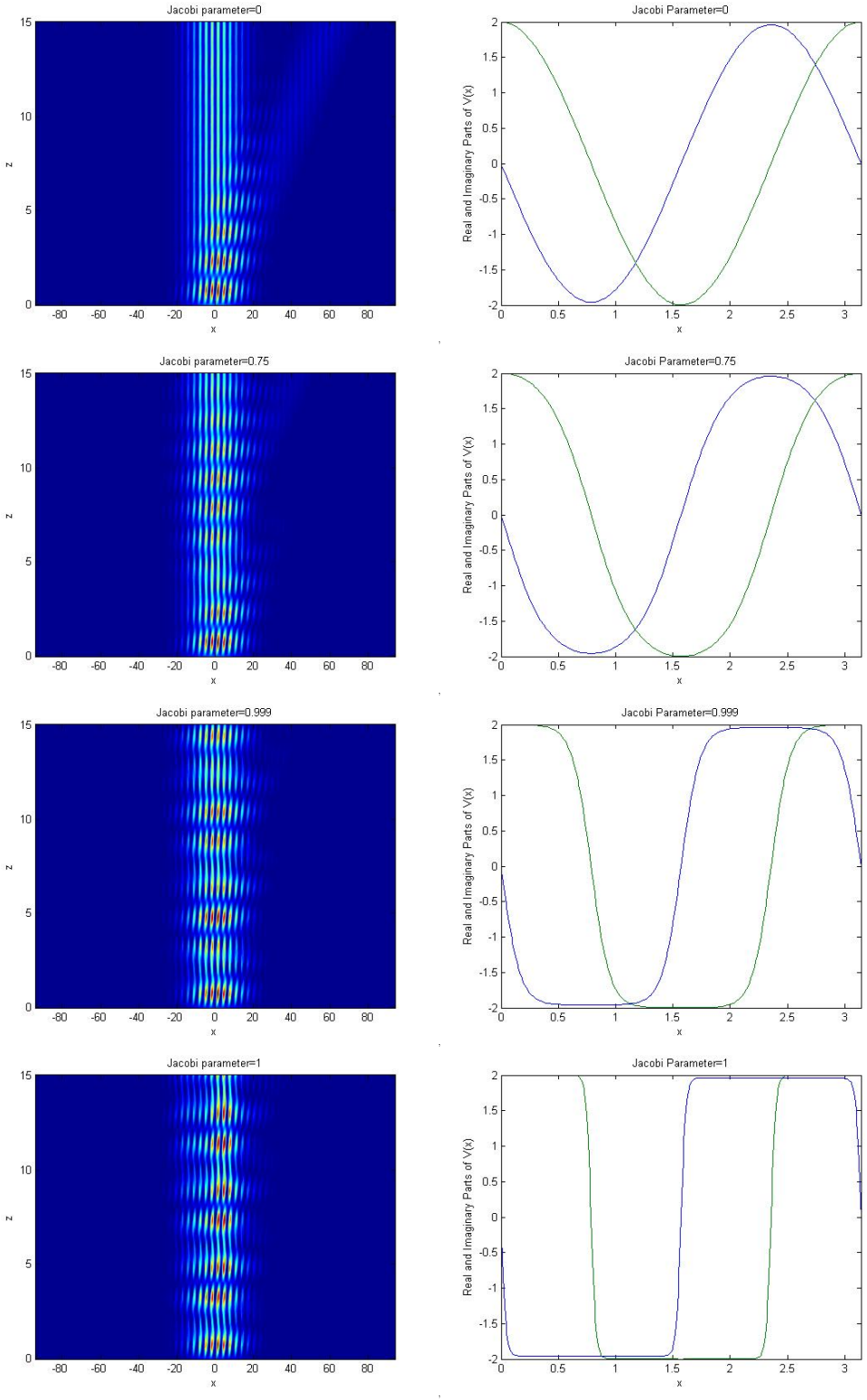

Figure 11: Intensity evolution for elliptic function potentials. Double diffraction appears to dissapear as the potential (right) changes from a sinusoidal (top) to a square-wave function (bottom). The real part of the potential is drawn in green and the imaginary part in blue.

3.6 Soliton Solutions in a Nonlinear $\mathcal{PT}$ Lattice

In a nonlinear $\mathcal{PT}$ lattice the beam dynamics obey the equation:

$$i\partial_z\psi(x,z) + \partial_x^2\psi(x,z) + V(x)\psi(x,z) + |\psi(x,z)|^2\psi(x,z) = 0 \tag{66}$$

Solitons are localised self-supported wave-packets that propogate at a constant speed. They are generally the result of a cancellation of dispersive and nonlinear phenomena. In the 2008 paper, *Optical Solitons in $\mathcal{PT}$ Periodic Potentials* [20], Christodoulides *et al.* demonstrate through numerical simulations that optical soliton solutions are supported in 1d and 2d periodic geometries. The potential employed is, the now familiar:

$$V(x) = \cos^2(x) + iV_0\sin(2x),$$

and it is made 2 dimensional simply by writing:

$$V(x,y) = \cos^2(x) + \cos^2(y) + iV_0[\sin(2x) + \sin(2y)] \tag{67}$$

Soliton solutions are sought in the form $\psi(x,z) = \phi(x)e^{i\beta z}$, where β is the propogation constant, and $\phi(x)$ is the nonlinear eigenmode. Under such conditions $\phi(x)$ satisfies:

$$\phi'' + V(x) + |\phi|\phi = \lambda\phi \tag{68}$$

An important issue when considering soliton solutions is their stability. This is modelled by considering infinitesimal perturbations of the solutions to (66) in the form:

$$\psi(x,z) = \phi(x)e^{i\beta z} + \epsilon[F(x)e^{i\sigma z} + G^*(x)e^{-i\sigma^* z}]e^{i\beta z} \tag{69}$$

with $\epsilon \ll 1$. $F(x)$ and $G(x)$ are the perturbation eigenfunctions, and σ indicates the perturbation growth rate. It is shown in reference [20] that if σ is real the solitons are stable, but if σ contains an imaginary part they are unstable.

The stability of each solution was tested in numerical simulations by introducing random noise on both the amplitude and the phase. Below the linear threshold $V_0 = 0.5$, stationary solitons were found to exist with real propogation constants. The instability of the solitons was found to increase with V_0. Furthermore, narrower beams appeared more stable and this is attributed to the enhancement of the index guiding by the nonlinearity, which is said to perturb the local $\mathcal{PT}$ transition value. Real propogation values exist for eigenmodes above threshold, however, these are found to correspond to unstable soliton solutions.

4 Conclusion

In summary, the work of Bender *et al.* found that non-Hermitian Hamiltonians have entirely real eigenspectra, provided they commute with, and share common eigenfunctions with, the PT operator. A threshold was identified in some Hamiltonians, above which, eigenfunctions of the Hamiltonian cease to be eigenfunctions of the PT operator, even though $[H, PT] = 0$ is valid, and the eigenspectrum of the Hamiltonian becomes complex. Such a transition, from a $\mathcal{PT}$-symmetric to a broken symmetry phase, was indeed witnessed when Christodoulides *et al.* experimentally implemented an optical realisation of $\mathcal{PT}$-symmetry in a linear coupled two-channeled system, in which the beam dynamics obeyed Schrödinger-like equations. These, and subsequent results, have been demonstrated here, aided by the use of MATLAB and Maple simulations.

The linear $\mathcal{PT}$-symmetric coupled system was shown to be nonreciprocal, owing to the skewed basis formed by the eigenfunctions of the non-Hermitian Hamiltonian. In the nonlinear version, the nonreciprocity was shown in cases to be be drastic, and for waveguides longer than some critical value, z_d, the intensity is seen to go exponentially to zero in the loss channel, irrespective of the input state. As a result of this property the system was discussed as a possible optical diode. The potential $4[\cos(x)^2 + iV_0 \sin(2x)]$ was considered extensively in the context of $\mathcal{PT}$-symmetric optical lattices, and, following private communication with Dr. H. F. Jones, an equivalent Hermitian Hamiltonian was presented. $\mathcal{PT}$-symmetric optical lattices were found to exhibit properties with no analog in real-potential systems, such as band merging, nonreciprocity, power oscillations, double refraction and phase transitions. Further communication with Dr. H. F. Jones permitted the inclusion of an apparent double refraction dependence on the sinusoidal shape of the potential, and graphical demonstrations were presented accordingly. Stationary soliton solutions were found to exist in nonlinear $\mathcal{PT}$ lattices, and their stabilities were

examined. Instability was found to increase with non-Hermiticity parameter V_0.

References

[1] C. M. Bender and S. Boettcher, Phys. Rev. Lett. **80**, (1998) 5243;

[2] C. M. Bender, D. C. Brody, and H. F. Jones, Phys. Rev. Lett. **89**, (2002) 270401; C. M. Bender, Am. J. Phys. **71**, (2003) 1095 ; Z. Ahmed, Phys. Lett. A **282** (2001), 343; B. Bagchi and C. Quesne, Phys. Lett. A **273** (2000), 285; H. Markum, R. Pullirsch, and T. Wettig, Phys. Rev. Lett. **83**, (1999) 484 .

[3] C. M. Bender, D. C. Brody, and H. F. Jones, Phys. Rev. Lett. **89**, (2002) 270401.

[4] C. M. Bender, Rep. Prog. Phys. **70**,(2007) 947-1018.

[5] S. Weigert S, Phys. Rev. A **68** (2003) 062111.

[6] D. N. Christodoulides, F. Lederer, and Y. Silberberg, Nature (London) **424**, (2003) 817.

[7] M. V. Berry and H. J. ODell, J. Phys. A 31, 2093 (1998); M. V. Berry, J. Phys. A **31**, (1998) 3493 .

[8] D. O. Chudesnikov and V. P. Yakovlev, Laser Phys. **1**, (1991) 110; M. K. Oberthaler *et all*., Phys. Rev. Lett. **77**, (1996) 4980; C. Keller et al., Phys. Rev. Lett. **79**, (1997) 3327.

[9] R. El-Ganainy, K. G. Makris, D. N. Christodoulides and Ziad H. Musslimani, Opt. Lett, **32**,(2007) 2632-2634.

[10] C. E Ruter, K. G. Makris, R. El-Ganainy, D. N. Christodoulides, M. Segev, and D. Kip, Nature Phys. **6**, (2010) 192

[11] H. Ramezani, T. Kottos, R. El-Ganainy and D. N. Christodoulides, arXiv:1005.5189v1, (2010)

[12] B. E. A. Saleh and M. C Teich, *Fundamentals of Photonics* (Wiley, 1991)

[13] S. M. Jensen, IEEE J. Q. Electron. **18**, (1982) 1580 ; V. M. Kenkre, D. K. Campbell, Phys. Rev. B **34**, (1986) 4959

[14] P. LiKamWa, *et al*, Electron. Lett. **21**, (1985) 26; U. Das, Y. Chen, and P. Bhattacharya, Appl. Phys. Lett. **51**, (1987) 1679.

[15] Z. H. Musslimani, K. G. Makris, R. El-Ganainy and D. N. Christodoulides, J. Phys. A **41**, (2008) 244019

[16] K. G. Makris, R. El-Ganainy and D. N. Christodoulides, Phys. Rev. Lett. **100**, (2008) 103904

[17] C. M. Bender, H. F. Jones and R. J. Rivers, Phys. Lett. **B 625**, (2005) 333

[18] M. Abramowitz and I. A. Stegun, *Handbook of Mathematical Tables*, Dover, New York 1970

[19] A. Mostafazadeh, J. Math. Phys. (N.Y.) **43**, (2002) 205

[20] Z. H. Musslimani, K. G. Makris, R. El-Ganainy and D. N. Christodoulides, Phys. Rev. Lett **100**, 2008 030402

Appendices

A Maple Code for 3d Plots of Linear System in Figures 1, 2, 3

First of all the following functions are defined:

$> xi(z) := sqrt(z^2 * (-4 * kappa^2 + gamma^2)) :$
$> E[1](z) := (cosh((xi(z))/(2)) + (gamma * z * sinh((xi(z))/(2)))/(xi(z))) * E[1](0) + 2 * I * ((z * sinh((xi(z))/(2)))/(xi(z)) * kappa) * E[2](0) : E[2](z) := (-cosh((xi(z))/(2)) + (gamma * z * sinh((xi(z))/(2)))/(xi(z))) * E[2](0) + 2 * I * ((z * sinh((xi(z))/(2)))/(xi(z)) * kappa) * E[1](0) :$
$> i[1](z) := abs(E[1](z))^(2) : i[2](z) := abs(E[2](z))^(2) :$
$> h := piecewise(x > 1, sin(Pi * x)) : g := piecewise(x < 1, -sin(Pi * x)) :$

Then the 3d plots are generated as an array in the *with(plots)* package:

$> with(plots) :$
$> B := Array(1..3, 1..2) :$
$> B[1,1] := plot3d(h * (eval(eval(i[1](z)/(i[1](z) + i[2](z)), gamma = 2 * kappa * alpha), [alpha = 0, kappa = 1.9, E[1](0) = 1, E[2](0) = 0])) + g * (eval(eval(i[2](z)/(i[1](z) + i[2](z)), gamma = 2 * kappa * alpha), [alpha = 0, kappa = 1.9, E[1](0) = 1, E[2](0) = 0])), z = 0..5, x = 0..2, scaling = constrained, orientation = [45, -60, 180]);$
$B[1,2] := plot3d(h * (eval(eval(i[1](z)/(i[1](z) + i[2](z)), gamma = 2 * kappa * alpha), [alpha = 0, kappa = 1.9, E[1](0) = 0, E[2](0) = 1])) + g * (eval(eval(i[2](z)/(i[1](z) + i[2](z)), gamma = 2 * kappa * alpha), [alpha = 0, kappa = 1.9, E[1](0) = 0, E[2](0) = 1])), z = 0..5, x = 0..2, scaling = constrained, orientation = [45, -60, 180]);$

$B[2,1] := plot3d(h * (eval(eval(i[1](z)/(i[1](z) + i[2](z)), gamma = 2 * kappa * alpha), [alpha = 1/2, kappa = 1.9, E[1](0) = 1, E[2](0) = 0]))+g*(eval(eval(i[2](z)/(i[1](z)+ i[2](z)), gamma = 2 * kappa * alpha), [alpha = 1/2, kappa = 1.9, E[1](0) = 1, E[2](0) = 0])), z = 0..5, x = 0..2, scaling = constrained, orientation = [45, -60, 180]);$

$B[2,2] := plot3d(h * (eval(eval(i[1](z)/(i[1](z) + i[2](z)), gamma = 2 * kappa * alpha), [alpha = 1/2, kappa = 1.9, E[1](0) = 0, E[2](0) = 1]))+g*(eval(eval(i[2](z)/(i[1](z)+ i[2](z)), gamma = 2 * kappa * alpha), [alpha = 1/2, kappa = 1.9, E[1](0) = 0, E[2](0) = 1])), z = 0..5, x = 0..2, scaling = constrained, orientation = [45, -60, 180]);$

$B[3,1] := plot3d(h * (eval(eval(i[1](z)/(i[1](z) + i[2](z)), gamma = 2 * kappa * alpha), [alpha = 1.2, kappa = 1.9, E[1](0) = 1, E[2](0) = 0]))+g*(eval(eval(i[2](z)/(i[1](z)+ i[2](z)), gamma = 2*kappa*alpha), [alpha = 1.2, kappa = 1.9, E[1](0) = 1, E[2](0) = 0])), z = 0..5, x = 0..2, scaling = constrained, orientation = [45, -60, 180]);$

$B[3,2] := plot3d(h * (eval(eval(i[1](z)/(i[1](z) + i[2](z)), gamma = 2 * kappa * alpha), [alpha = 1.2, kappa = 1.9, E[1](0) = 0, E[2](0) = 1]))+g*(eval(eval(i[2](z)/(i[1](z)+ i[2](z)), gamma = 2*kappa*alpha), [alpha = 1.2, kappa = 1.9, E[1](0) = 0, E[2](0) = 1])), z = 0..5, x = 0..2, scaling = constrained, orientation = [45, -60, 180]) :$

$display(B);$

B Maple Code for Plots of Analytic Solution for Intensity at Output in Figure 4

The following analytic solutions are defined:

$> xi(z) := sqrt(z^2 * (-4 * kappa^2 + gamma^2)) :$

$> E[1](z) := (cosh((xi(z))/(2)) + (gamma * z * sinh((xi(z))/(2)))/(xi(z))) * E[1](0) + 2 * I * ((z * sinh((xi(z))/(2)))/(xi(z)) * kappa) * E[2](0) : E[2](z) := (-cosh((xi(z))/(2)) + (gamma * z * sinh((xi(z))/(2)))/(xi(z))) * E[2](0) + 2 * I * ((z * sinh((xi(z))/(2)))/(xi(z)) * kappa) * E[1](0) :$

$> i[1](z) := abs(E[1](z))^(2) : i[2](z) := abs(E[2](z))^(2) :$

Having defined the functions they are evaluated ats z=2 and kappa=2, before plotted in a plot array as functions of T.

$> f1 := eval(eval(i[2](z)/(i[1](z)+i[2](z)), gamma = (5/2)*kappa*(1-exp(T))), [z = 2, kappa = 2, E[1](0) = 1, E[2](0) = 0]) :$

$f2 := eval(eval(i[1](z)/(i[1](z)+i[2](z)), gamma = (5/2)*kappa*(1-exp(T))), [z = 2, kappa = 2, E[1](0) = 1, E[2](0) = 0]) :$

$> f3 := eval(eval(i[2](z)/(i[1](z)+i[2](z)), gamma = (5/2)*kappa*(1-exp(T))), [z = 2, kappa = 2, E[1](0) = 0, E[2](0) = 1]) :$

$f4 := eval(eval(i[1](z)/(i[1](z)+i[2](z)), gamma = (5/2)*kappa*(1-exp(T))), [z = 2, kappa = 2, E[1](0) = 0, E[2](0) = 1]) :$

$> fs := Array(1..2);$

$fs[1] := plot([f1, f2], T = 0..2, title = typeset("CHANNEL1EXCITED"), labels = [T, i[1, 2]/(i[1] + i[2])]) :$

$fs[2] := plot([f3, f4], T = 0..2, title = typeset("CHANNEL2EXCITED"), labels = [T, i[1, 2]/(i[1] + i[2])]) : display(fs);$

C Maple Code for Band Structure in Figure 7

For the potentials defined below the equations are solved for k using the Floquet method after solving the dynamical equations numericaly for a specified value of β using the Runge Kutta method. This process is repeated in increment steps of β that provide k values between ± 1. The inverted graph is then plotted as points joined by a line, with both graphs displayed together. This produces the left hand picture in Figure 7.

$> V03(x) := 4 * (cos(x)^2 + 0.3 * I * sin(2 * x)) :$

$> V05(x) := 4 * (cos(x)^2 + 0.5 * I * sin(2 * x)) :$

$> for\ i\ to\ 61\ do\ beta[i] := 2.5 - 0.075 * (i - 1)\ end\ do :$

$> betavalues := Vector(61, (i) - Re(beta[i])) :$

$> kvalues03 := Vector(61, (i) -> Re(evalf[5](arccos(Re(1/2 *$

$(subs(dsolve(\{diff(U[1](x), `\$`(x, 1)) = Up[1](x), diff(Up[1](x), `\$`(x, 1)) = (beta[i] -$

$V03(x)) * U[1](x)\} union \{U[1](0) = 1, Up[1](0) = 0\}, numeric, output =$

$listprocedure, method = rkf45, range = -Pi..Pi), U[1](x))(Pi) +$

$subs(dsolve(\{diff(U[2](x), `\$`(x, 1)) = Up[2](x), diff(Up[2](x), `\$`(x, 1)) = (beta[i] -$

$V03(x)) * U[2](x)\} union \{U[2](0) = 0, Up[2](0) = 1\}, numeric, output =$

$listprocedure, method = rkf45, range = -Pi..Pi), Up[2](x))(Pi))))/Pi))) :$

$> kvalues05 := Vector(61, (i) -> Re(evalf[5](arccos(Re(1/2 *$

$(subs(dsolve(\{diff(U[1](x), `\$`(x, 1)) = Up[1](x), diff(Up[1](x), `\$`(x, 1)) =$

$(beta[i] - V05(x)) * U[1](x)\} union \{U[1](0) = 1, Up[1](0) = 0\}, numeric, output =$

$listprocedure, method = rkf45, range = -Pi..Pi), U[1](x))(Pi) +$

$subs(dsolve(\{diff(U[2](x), `\$`(x, 1)) = Up[2](x), diff(Up[2](x), `\$`(x, 1)) = (beta[i] -$

$V05(x)) * U[2](x)\} union \{U[2](0) = 0, Up[2](0) = 1\}, numeric, output =$

$listprocedure, method = rkf45, range = -Pi..Pi), Up[2](x))(Pi))))/Pi))) :$

$> plota := plot([< kvalues03 | betavalues >, < -kvalues03 | betavalues >], color =$

$red)$:

$plotb := plot([< kvalues05|betavalues >, < -kvalues05|betavalues >], color = green)$:

$> display(\{plota, plotb\}, labels = ['k', 'beta(k)'])$;

D MATLAB Code for Intensity Evolutions in Figures 8, 9, 10, and 11

This program features the split-operator method (Appendix F) and a fast Fourier transform.

```
function FieldIntensity


clear all


%variables:
v0=0.49;
%w=input ('Input width of Gaussian    ');
 w=6;
 jp=input('Input Jacobi parameter ');


%x and k grid and timesteps:
xmin=-30*pi;xmax=30*pi; % x-width
N=2^11; hx=(xmax-xmin)/N
kmax=pi/hx; hk=2*kmax/N  % k-width


% theta=2*(pi/180);  %Beam incident at an angle
% kk=input('Input k/kmax   ');
% kk=kmax*kk;


dt=0.001;ntime=15000;  %timesteps


% Propagators for potential and kin. energy:
```

```
x=zeros(1,N);
expv=zeros(1,N);
for j=1:N
    x(j)=xmin+hx*(j-1);
    expv(j)=exp(-1i*potf(x(j),v0,jp)*dt/2);
end
p=zeros(1,N);
expt=zeros(1,N);
for j=1:N
    k=-kmax+hk*(j-1);
    p(j)=k;
    ekin=k^2;
    expt(j)=exp(-1i*ekin*dt);
end



%initial 'wavepacket':
psi=zeros(1,N);
 for j=1:N
    % if x(j)>=-pi && x(j)<=pi
     %psi(j)=1;                    %Single channel
      %end
      psi(j)=exp(-(x(j)/(w*pi))^2);%*exp(-1i*x(j)*kk*sin(theta)); %Gaussian
 end
% psi=ones(1,N);        %Constant

checki=0;
for j=1:N
```

```
    checki=checki+conj(psi(j))*psi(N+1-j);
end
checki
%%%%%%%%%%%%%%%%%%%%%%%%%%%%%%%%%%%%%%%%%%%%%%%%%%%%%%%%%%%%%%%%%%%%%%%%
% Somehow check doesn't work as soon as theta is non zero! %
% Certainly checki then becomes artificially small         %
%%%%%%%%%%%%%%%%%%%%%%%%%%%%%%%%%%%%%%%%%%%%%%%%%%%%%%%%%%%%%%%%%%%%%%%%

%initialise vectors to store time and amplitude:
time=zeros(ntime+1,1);
X=zeros(N,ntime);
time(1)=0;

%time propagation:
exptshift=fftshift(expt);
for n=1:ntime
    time(n+1)=time(n)+dt;
    psi=expv.*fftshift(ifft(exptshift.*fft(fftshift(expv.*psi))));
    X(:,n)=abs(psi).^2;
end
%Note that .* stands for element-by-element multiplication
checkf=0;
    for j=1:N
        checkf=checkf+conj(psi(j))*psi(N+1-j);
    end
    checkf
    check=(checkf-checki)/(checkf+checki)
```

```
figure
imagesc(x,time,X.')
set(gca,'YDir','normal')
xlabel('x')
ylabel('z')
title(['Jacobi parameter=', num2str(jp)])
%title=(['w=',num2str(w)])
%title('Single channel')
%title(['Fig 3(b) :k/kmax=',num2str(kk/kmax])

function y=potf(x,v0,jp)
% y=4*(cos(x)^2+1i*v0*sin(2*x));
y=2*(-ellipj((4*x/pi -1)*ellipke(jp),jp)
    +2i*v0*ellipj(4*x*ellipke(jp)/pi,jp));
return
```

E MATLAB Code for Plots of Elliptic Functions in Figure 11

```
function EllipPlot


clear all
%variables:
v0=0.49;
jp=input('Input Jacobi parameter     ');
fplot(@ (x) [-4*v0*ellipj(4*x*ellipke(jp)/pi,jp),
         2*(-ellipj((4*x/pi -1)*ellipke(jp),jp))] , [0 pi]);
xlabel('x')
ylabel(' Real and Imaginary Parts of V(x) ')
title(['Jacobi Parameter=', num2str(jp)])
```

F The Split-Operator Method and the FFT (as used in Appendix D)

The split-operator method enables an accurate approximation of an operator. In this case we have that the time evolution of a state may be written:

$$\psi(x, t+\epsilon) = e^{-i\hat{H}\epsilon}\psi(x,t) \tag{70}$$

with $\epsilon = \delta t$ some infinitesimal time, later than time t. For reasons that will be explained it is now advantageous to split the operator, $\hat{H}$, into $\hat{p}^2 + V(x)$, such that (70) becomes:

$$\psi(x, t+\epsilon) = e^{-i(\hat{p}^2+V(x))\epsilon}\psi(x,t) \tag{71}$$

The split operators in general do not commute, and consequently, the commutator will feature in the Taylor expansion of the exponential. An accurate approximation of the operator $e^{-i(\hat{p}^2+V(x))\epsilon}$, with error $\mathcal{O}(\epsilon^3)$, exists in the form of:

$$e^{-i(\hat{p}^2+V(x))\epsilon} = e^{-\frac{i}{2}V(x)\epsilon}e^{-i\hat{p}^2\epsilon}e^{-\frac{i}{2}V(x)\epsilon} + \mathcal{O}(\epsilon^3) \tag{72}$$

Proof: Expand left and right hand sides of (72):

$$\begin{aligned} LHS &= 1 - i(\hat{p}^2 + V(x))\epsilon - 1/2(\hat{p}^2 + V(x))^2\epsilon^2 + \mathcal{O}(\epsilon^3) \qquad (73)\\ &= 1 - i(\hat{p}^2 + V(x))\epsilon - 1/2(\hat{p}^4 + V(x)^2 + \hat{p}^2V(x) + V(x)\hat{p}^2)\epsilon^2 + \mathcal{O}(\epsilon^3) \end{aligned}$$

$$\begin{aligned} RHS &= (1 - i/2V(x)\epsilon - 1/8V(x)^2\epsilon^2)(1 - i\hat{p}^2\epsilon - 1/2\hat{p}^4\epsilon^2)(1 - i/2V(x)\epsilon - 1/8V(x)^2\epsilon^2)\\ &\quad +\mathcal{O}(\epsilon^3) \qquad (74)\\ &= 1 - i(\hat{p}^2 + V(x))\epsilon - 1/2(\hat{p}^4 + V(x)^2 + \hat{p}^2V(x) + V(x)\hat{p}^2)\epsilon^2 + \mathcal{O}(\epsilon^3) \end{aligned}$$

Both the left and right hand sides of (72) are the same and this completes the proof. The advantage of writing equation (70) in the form:

$$\psi(x, t+\epsilon) = e^{-\frac{i}{2}V(x)\epsilon} e^{-i\hat{p}^2\epsilon} e^{-\frac{i}{2}V(x)\epsilon} \psi(x, t), \tag{75}$$

is that it is now possible to multiply the two functions of x on the right of (75), i.e. $e^{-\frac{i}{2}V(x)\epsilon}\psi(x,t)$, in an element-by-element efficient manner in MATLAB. If then a Fourier transform is performed so that the result is a function of p a similar multiplication is possible with $e^{-i\hat{p}^2\epsilon}$. Finally, after inverse transforming back to a function of x, that result is multiplied by the first function, $e^{-\frac{i}{2}V(x)\epsilon}$. Algorithms exist for a fast Fourier transform (FFT) that make this process computationaly efficient.